Rapid Communications | Editors' Suggestion

Extensional rheology of a dilute particle-laden viscoelastic solution

Anika Jain, Jonas Einarsson, and Eric S. G. Shaqfeh*
Department of Chemical Engineering, Stanford University, Stanford, California 94305, USA

(Received 5 April 2019; published 9 September 2019)

Recent discoveries have allowed a mathematical and computational foundation for understanding the rheology of particles suspended in viscoelastic fluids. We employ these new tools to understand the extensional rheology of such suspensions. We accomplish this by first calculating the renormalized particle contribution to the extensional viscosity in such a suspension in the dilute particle limit over a wide range of extensional Weissenberg number and Hencky strain. The models we use for the suspending fluids are the simplest dumbbell models—the Oldroyd-B, FENE-P, and Giesekus models—such that our results are general for polymer solutions which exhibit strong strain hardening at values of the Weissenberg number above those which engender the coil-stretch transition, $\mathrm{Wi} \geqslant 0.5$. We demonstrate that the effect of particles on the "extra elongational viscosity" relative to the fluid is nonmonotonic in strain (increasing for small strain and then decreasing for large strain). Thus at a fixed strain, the particle "extra viscosity" relative to the fluid may increase or decrease with Wi. We demonstrate that this interesting behavior is due to the interplay between the two contributions of the "particle-induced fluid stress" (PIFS) and the "stresslet" to the extra viscosity. The contribution of the particle-induced fluid stress to the suspension viscosity increases at small strain but plateaus and then decreases at higher values of the strain. Thus, at small strain the local velocity gradients near a particle increase the polymer stretch, while for greater strain, polymers which have undergone the coil-stretch transition collapse in the neighborhood of a given particle. On the other hand, the stresslet contribution to the viscosity relative to the fluid decreases monotonically as the polymer stretch surrounding a given particle "shields" the particle and thus reduces the local surface tractions. Beyond Hencky strain of approximately 2 the decreasing value of the stresslet coupled with the plateauing of the PIFS, causes the overall reduction in the particle-induced extra viscosity relative to that of the fluid.

DOI: 10.1103/PhysRevFluids.4.091301

I. INTRODUCTION

The presence of strong strain hardening in polymer solutions is one of their most important rheological characteristics [1–4]. Thus the extensional viscosity of a polymer solution, at sufficiently large strain rates and Hencky strain, can be orders of magnitude larger than the solvent alone. The control of processing flows of these materials is essentially dictated by this strain hardening [1–4], which has historically been associated with the famous coil-stretch transition of the individual polymer chains [5–7]. In the last 20 years, this connection has been made unambiguous by the simultaneous measurement of the extensional viscosity of DNA solutions and microscopy of the molecular configuration [8–13]. Strain hardening and the coil-stretch transition is still a very active area of research with a number of groups seeking to understand the effect of intermolecular interactions on the coil-stretch transition. The direct application of these rheological studies ranges

*esgs@stanford.edu

from extrusion molding to fiber spinning. However a great many of the associated practical materials contain particle additives; they are hence *a suspension in a viscoelastic fluid*. These suspensions play key roles in many energy applications (e.g., fracking fluids) [14], materials design applications (e.g., injected composite materials, pastes, and paints) [15], and consumer product applications (liquid medicines and drugs).

Recently, there have been very significant advances in understanding the *shear* rheology of particle suspensions in highly elastic solutions [16–21]. Indeed the most salient experimental feature in this regard is the strong shear thickening of the suspensions (both in the viscosity and the primary normal stress coefficient), which is entirely absent in the fluids alone [18,19,22–24]. These advances include (a) methods for renormalization of the long-range interactions in these suspensions, such that dilute suspension theory could be applied [18–20,25], (b) the first calculation of the dilute limiting shear viscosity for a suspension of spheres for "weak flow" using these renormalizations, (c) accurate large-scale computations of the renormalized shear flow rheological quantities beyond the weak flow limit [19–21], and (d) qualitative reproduction of the experiments [21]. It is the purpose of this Rapid Communication to apply these advances to an understanding of the extensional rheology of particle suspensions in a viscoelastic polymer solution. Previous studies [26–28] focus on two-dimensional inertialess particle suspensions in Newtonian or viscoelastic fluids under planar elongational flows. In this study, we present three-dimensional (3D) numerical results for a dilute viscoelastic suspension of spherical particles in uniaxial extension. We perform 3D simulations to ensure elastic instabilities do not develop during evolution of polymeric flow with time.

II. PROBLEM FORMULATION

A. Bulk stress in a viscoelastic suspension

The general averaging procedure to obtain the macroscopic stress in a suspension of rigid particles has been discussed in [16,19,20,29,30]. Here, we give a very brief recapitulation of the method. The bulk stress in a suspension can be obtained by averaging over a sufficiently large volume with the volume averaged velocity field matching the ensemble averaged velocity field and this is equivalent to the ensemble average [29] for a statistically homogeneous suspension. Thus the "bulk" stress defined in terms of the volume average is

$$\overline{\sigma_{ij}} = \frac{1}{V}\int_V \sigma_{ij} dV, \tag{1}$$

where the overbar denotes volume average and V is the total suspension (particles and fluid) volume. If the stress contributions from the particle phase σ_{ij}^p and the fluid phase σ_{ij}^f are separated and furthermore, if the stress contributions due to suspending fluid without any particles σ_{ij}^{f0} and the stress contributions due to particles are made distinct, then as shown in [18–20], Eq. (1) becomes

$$\overline{\sigma_{ij}} = \sigma_{ij}^{f0} + n\left[\int_{V_1} \left(\sigma_{ij}^f - \sigma_{ij}^{f0}\right) dV + \int_{A_1} x_j \sigma_{ik}^f n_k dA\right], \tag{2}$$

where diluteness has been assumed and the total particle contribution to the stress is obtained by multiplying the number density of particles n in suspension with the per particle contribution. In the above equation, V_1 is the domain volume that contains a single particle and is large enough such that any disturbance due to the particle decays far from the particle and at the boundaries of the domain. The symbol A_1 represents a single-particle surface and n_k is the unit normal vector pointing out of the particle surface. The number density n is related to particle volume fraction ϕ as $n = \frac{\phi}{V_p}$ where V_p is the volume of a single particle. The per particle contribution to the extension viscosity η_E^p is then the sum of contributions from the particle-induced fluid stress (PIFS) Σ_{ij} and the stresslet S_{ij},

viz.,

$$\Sigma_{ij} = \frac{1}{V_p}\int_{V_1}\left(\sigma_{ij}^{f} - \sigma_{ij}^{f0}\right)dV; \quad S_{ij} = \frac{1}{V_p}\int_{A_1} x_j \sigma_{ik}^{f} n_k dA. \tag{3}$$

Assuming that the flow is homogeneous, steady uniaxial extensional flow, where the rate of strain tensor $E_{ij} = \dot{\epsilon}[\delta_{i1}\delta_{j1} - \frac{1}{2}(\delta_{i2}\delta_{j2} + \delta_{i3}\delta_{j3})]$, we can define a per particle contribution to the extensional viscosity of the suspension η_E^{ϕ} through the relation

$$\eta_E^{p}\dot{\epsilon} = \left(\Sigma_{11} - \frac{\Sigma_{22} + \Sigma_{33}}{2}\right) + \left(S_{11} - \frac{S_{22} + S_{33}}{2}\right). \tag{4}$$

The total suspension viscosity for any dilute volume fraction ϕ follows directly from Eq. (2) after the definition of particle viscosity is substituted and the particle number density is replaced by the volume fraction,

$$\eta_E^{\phi} = \eta_E^{\phi=0} + \phi\eta_E^{p}, \tag{5}$$

where $\eta_E^{\phi=0}\dot{\epsilon} = \sigma_{11}^{f0} - \frac{1}{2}(\sigma_{22}^{f0} + \sigma_{33}^{f0})$ and therefore $\eta_E^{\phi=0}$ is the extensional viscosity of the suspending fluid. After rearranging, we obtain an equation for the relative difference between suspension and suspending fluid extensional viscosity,

$$\frac{\eta_E^{\phi}}{\eta_E^{\phi=0}} - 1 = \phi\frac{\eta_E^{p}}{\eta_E^{\phi=0}}, \tag{6}$$

which can be calculated in dilute simulations by computing the ratio of particle viscosity to fluid viscosity.

B. Governing equations

We consider a neutrally buoyant sphere placed at the center of a rectangular computation domain $(\pm L_1/2, \pm L_2/2, \pm L_3/2)$ in a mean flow field $\overline{u_i} = (\dot{\epsilon}x, -\dot{\epsilon}y/2, -\dot{\epsilon}z/2)$ where $\dot{\epsilon}$ is the extension rate. The mean flow is imposed on the walls of the domain far from the particle. There is no net force or torque on the sphere due to the symmetric nature of the imposed flow. The dimensionless governing equations are

$$\frac{\partial u_i'}{\partial x_i'} = 0; \quad \mathrm{Re}\left(\frac{\partial u_i'}{\partial t'} + u_j'\frac{\partial u_i'}{\partial x_j'}\right) = -\frac{\partial p'}{\partial x_i'} + \frac{\partial \sigma_{ij}^{f'}}{\partial x_j'}, \tag{7}$$

where the prime denotes a nondimensional variable. Length is made dimensionless by particle radius a, time by inverse extension rate $\dot{\epsilon}$, velocity by $\dot{\epsilon}a$, and stress by $\eta_0\dot{\epsilon}$ where η_0 is the zero shear viscosity of the suspending fluid. The fluid stress is the sum of Newtonian and polymer stress:

$$\sigma_{ij}^{f'} = \beta\left(\frac{\partial u_i'}{\partial x_j'} + \frac{\partial u_j'}{\partial x_i'}\right) + \tau_{ij}^{p'}, \tag{8}$$

where β is the ratio of Newtonian solvent viscosity to the zero shear viscosity and $\tau_{ij}^{p'}$ is the nondimensional polymer stress. The FENE-P equation describing the evolution of the polymer conformation tensor C_{ij} is

$$\frac{\partial C_{ij}}{\partial t'} + u_k'\frac{\partial C_{ij}}{\partial x_k'} - C_{ik}\frac{\partial u_j'}{\partial x_k'} - C_{jk}\frac{\partial u_i'}{\partial x_k'} = -\frac{1}{\mathrm{Wi}}\left(\frac{C_{ij}}{1 - \frac{C_{kk}}{L^2}} - \delta_{ij}\right), \tag{9}$$

where the conformation tensor components C_{ij} and the finite polymer extensibility L are nondimensionalized by the polymer radius of gyration. There are two dimensionless groups: the particle

Reynolds number defined as $\mathrm{Re} = \rho\dot{\epsilon}a^2/\eta_0$ and the Weissenberg number $\mathrm{Wi} = \lambda\dot{\epsilon}$ where λ is the longest polymer relaxation time. The polymer stress is related to the conformation tensor through

$$\tau_{ij}^{p'} = \frac{1-\beta}{\mathrm{Wi}}\left(\frac{C_{ij}}{1-\frac{C_{kk}}{L^2}} - \delta_{ij}\right). \tag{10}$$

When $L \to \infty$, the FENE-P equation is equivalent to the Oldroyd-B model. The Giesekus equation, in the same notation, is

$$\frac{\partial C_{ij}}{\partial t'} + u_k'\frac{\partial C_{ij}}{\partial x_k'} - C_{ik}\frac{\partial u_j'}{\partial x_k'} - C_{jk}\frac{\partial u_i'}{\partial x_k'} = -\frac{1}{\mathrm{Wi}}(C_{ij}-\delta_{ij}) - \frac{\alpha}{\mathrm{Wi}}(C_{ik}-\delta_{ik})(C_{kj}-\delta_{kj}), \tag{11}$$

where α is the mobility parameter. When $\alpha = 0$, the equation is again equivalent to the Oldroyd-B model. To complete a calculation of the full time-dependent problem, for any of these constitutive equations, we require initial conditions for the velocity and conformation tensor. For the initial velocity we choose the Newtonian creeping flow solution for flow past a sphere in uniaxial extensional flow, and for the initial conformation tensor we choose the identity tensor (the dimensionless, equilibrium configuration thus producing no polymer stress). We also impose the boundary condition on the conformation tensor such that the polymer conformation tensor at the walls of the domain takes values corresponding to suspending fluid at different strains and Wi. This is allowed because the simulation domain is taken to be big enough such that there is no disturbance due to particles at the walls of the domain. We drop the primes in the rest of the Rapid Communication for convenience and all the variables are assumed to be nondimensional.

C. Numerical simulations

The simulations are run using a massively parallel finite volume solver developed at Stanford and the details of the solver can be found in [19], and the references therein. The domain grid conforms to the body of a single sphere and is meshed using tetrahedral elements of size $a/60$ near the particle surface and bigger elements of size $a/40$ far from the particle. The simulations are run in the limit $\mathrm{Re} \ll 1$. The domain convergence is tested for all simulations and the results are found to vary by less than 5% between two domain sizes $(40a, 40a, 40a)$ and $(80a, 40a, 40a)$ where the longest dimension of the box is in the direction of principal extension of the flow, i.e., the "1" direction.

III. RESULTS AND DISCUSSION

We numerically compute the ratio of the per particle extensional viscosity to the fluid extensional viscosity as a function of strain for a range of Wi to study the effect of particles on the suspension viscosity. The ratio can be thought as the "Einstein coefficient" [31,32] for the startup of uniaxial extensional flow of spheres in a viscoelastic fluid.

A. Small strain results

To gain a physical understanding and test the accuracy of our numerical solutions, we first use perturbation theory at small strains to calculate the PIFS and stresslet analytically for the Oldroyd-B model. The polymer conformation tensor, fluid velocity, and pressure are expanded in the small strain ϵ in the usual manner:

$$C_{ij} = \delta_{ij} + \epsilon C_{ij}^{(1)} + \epsilon^2 C_{ij}^{(2)} + \cdots, \tag{12}$$

$$u_i = u_i^{(0)} + \epsilon u_i^{(1)} + \epsilon^2 u_i^{(2)} + \cdots, \tag{13}$$

$$p = p^{(0)} + \epsilon p^{(1)} + \epsilon^2 p^{(2)} + \cdots. \tag{14}$$

The leading order $O(1)$ flow field is the Newtonian field and the conformation tensor is equal to the identity tensor. Thus, there is no PIFS at $O(1)$ and the stresslet is given by $S_{ij}^{(0)} = 5E_{ij}$ where E_{ij} is the average rate of strain tensor in the fluid domain; this is in accord with the famous Einstein result [31,32]. At $O(\epsilon)$ the conformation tensor is proportional to the rate of strain of the Newtonian field. Thus, again at this order the deviatoric stress is proportional to the deviatoric Newtonian stress at $O(1)$ and thus there is an associated pressure correction but no additional velocity correction, viz.,

$$u_i^{(1)} = 0, \tag{15}$$

$$p^{(1)} = \frac{1-\beta}{\mathrm{Wi}} p^{(0)}, \tag{16}$$

$$C_{ij}^{(1)} = 2e_{ij}^{(0)}. \tag{17}$$

The fluid stress, at this order, is given by

$$\sigma_{ij}^{(1)} = \frac{1-\beta}{\mathrm{Wi}}\left(-p^{(0)}\delta_{ij} + 2e_{ij}^{(0)}\right) \tag{18}$$

and the stresslet correction then simply reflects the change in the viscosity:

$$S_{ij}^{(1)} = \frac{1-\beta}{\mathrm{Wi}} 5E_{ij}, \tag{19}$$

and there is no correction to the PIFS. Continuing, then the conformation tensor at $O(\epsilon^2)$ is given by

$$C_{ij}^{(2)} = -\frac{e_{ij}^{(0)}}{\mathrm{Wi}} - u_m^{(0)}\frac{\partial e_{ij}^{(0)}}{\partial x_m} + \dot{\gamma}_{ik}^{(0)} e_{jk}^{(0)} + \dot{\gamma}_{jk}^{(0)} e_{ik}^{(0)}, \tag{20}$$

where $e_{ij}^{(0)}$ is the local strain rate tensor and $\dot{\gamma}_{jk}^{(0)}$ is the local velocity gradient in the Newtonian flow. The flow field is now non-Newtonian at $O(\epsilon^2)$ and rather than determine the correct flow field, one can determine the stresslet correction using the reciprocal theorem [25]:

$$S_{ij}^{(2)} = \frac{1-\beta}{\mathrm{Wi}}\frac{3}{14}E_{ik}E_{kj} - \frac{1-\beta}{\mathrm{Wi}^2}5E_{ij}. \tag{21}$$

The $O(\epsilon^2)$ correction to the PIFS is calculated using the renormalized averaging procedure of [25]

$$\Sigma_{ij}^{(2)} = \frac{1-\beta}{\mathrm{Wi}}\frac{25}{7}E_{ik}E_{kj}. \tag{22}$$

We show the comparison of the small strain theory to our transient numerical simulation results for the stresslet and the PIFS in Fig. 1. The theory and simulations agree well at small strains but the theoretical prediction for the stresslet departs from the numerical simulations at strains $\epsilon \approx 10^{-1}$ and the small strain theory no longer holds. Moreover, in the inset to each figure, we see that the stresslet ratioed to the fluid stress decreases monotonically with strain, while the PIFS monotonically increases. This will be important in the physical description of our numerical results below.

B. Numerical results at finite strain and Weissenberg number

We performed the full 3D simulations to calculate the per particle extra viscosity compared to the fluid at finite strains and Wi. We modeled the suspending fluid using the FENE-P equation with parameters $\beta = 0.68, L = 100$ and also using the Oldroyd-B equation with the same value of $\beta = 0.68$. The parameters of the Giesekus model used are $\alpha = 10^{-3}, \beta = 0.68$. We used the value of viscosity ratio $\beta = 0.68$ in our simulations because the Giesekus model parameters $\beta = 0.68, \alpha = 0.0039$ fit the steady shear rheology of the Boger fluid used by Dai *et al.* [23] as shown

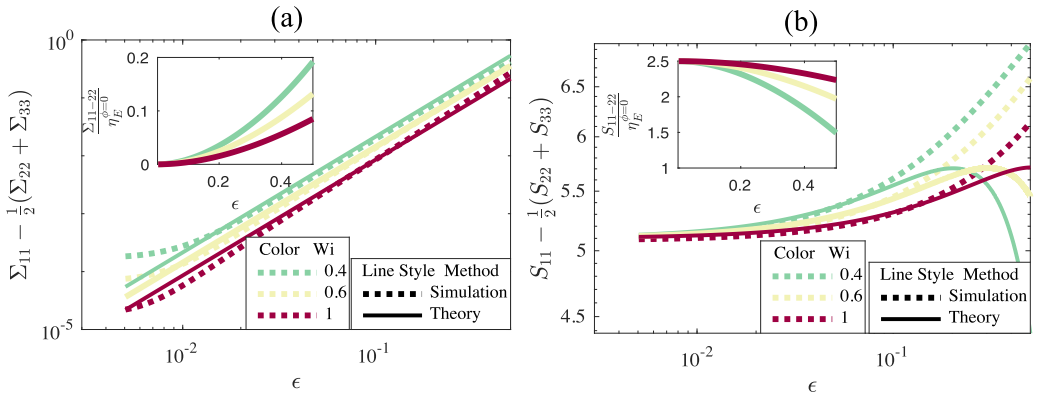

FIG. 1. Comparison of small strain theory with transient simulations as a function of strain for (a) stresslet and (b) particle-induced fluid stress. The parameter $\beta = 0.68$ for the Oldroyd-B model used in simulations.

in [19]. Each simulation is run for a total strain, $\dot{\epsilon}t$, of 7. Figure 2 shows the viscosity ratio with increasing Hencky strain for different models at a range of Wi. We also explore the effect of smaller $\beta = 0.4$ value on the ratio of particle viscosity to suspending fluid viscosity for the Oldroyd-B model at different Wi. The inset shows the viscosity ratio for the Oldroyd-B model and Wi $= 1$ at two different β values. The dotted line is for $\beta = 0.68$ and the dashed line is for $\beta = 0.4$. We see that the value of ratio (or Einstein's coefficient) is close to 2.5 for Wi $= 0.1$ at all values of strain for all models studied. Thus, we predict that the viscoelastic suspensions behave like Newtonian suspensions in the limit of small strain and Wi. However, the viscosity ratio is nonmonotonic in strain for other values of Wi considered in the study. The nonmonotonicity occurs for all model parameters studied, i.e., different values of L, α, and viscosity ratio β and more importantly for all polymer constitutive models. The inset in Fig. 2 shows that the value of the viscosity ratio for

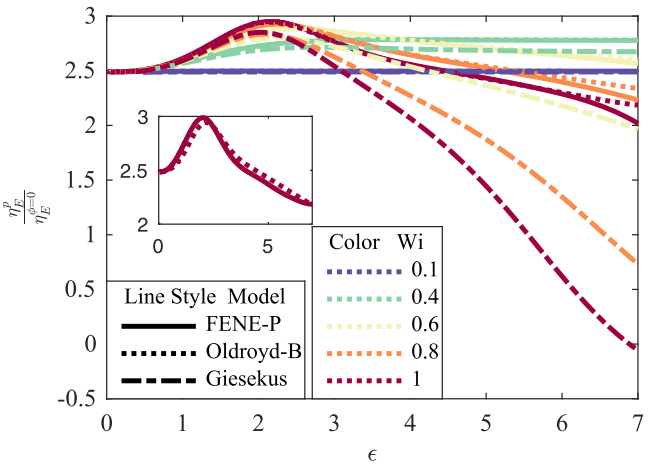

FIG. 2. Ratio of particle viscosity to suspending fluid viscosity with strain for a range of Weissenberg numbers for the FENE-P, Oldroyd-B, and Giesekus models. The parameters of the FENE-P model are $\beta = 0.68$, $L = 100$, of the Oldroyd-B model are $\beta = 0.68$, and of the Giesekus model are $\alpha = 10^{-3}$, $\beta = 0.68$. The inset also shows the ratio of particle viscosity to fluid viscosity for the Oldroyd-B model and Wi $= 1$. The two curves correspond to two different β values. The β value for the dotted curve is equal to 0.68 and the β value for the dashed curve is equal to 0.4. We see that β does not have a significant effect on the ratio.

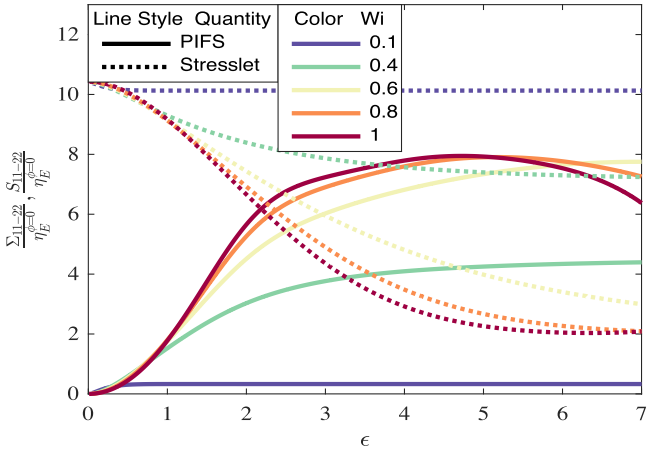

FIG. 3. Ratio of PIFS and stresslet to suspending fluid viscosity with strain for different Wi for the FENE-P model. The parameters of the FENE-P model used in simulations are $\beta = 0.68$, $L = 100$.

Wi $= 1$ is unaffected by the value of β and we have also seen very little effect of varying β at other values of Wi. We believe that this behavior is universal for spherical particles in dilute polymer solutions subject to (uniaxial) extensional flow. Furthermore, the viscosity ratio computed for both FENE-P and Oldroyd-B is identical until strains ≈ 6 after which the value of the finite extensibility parameter L makes a difference. The Giesekus model demonstrates lower values of the ratio of the particle viscosity to the fluid viscosity compared to the other two models starting from strains of about 2, but essentially demonstrates the same qualitative behavior.

The nonmonotonicity in particle viscosity relative to fluid can be attributed to the PIFS and stresslet contributions to the particle viscosity. Figure 3 shows the ratio of the PIFS and stresslet to suspending fluid viscosity as a function of strain for different Wi. We see that the ratio of the stresslet to the fluid viscosity decreases monotonically with strain (as it did in the small strain theory) but the ratio of PIFS to fluid viscosity is nonmonotonic with strain for all the Wi > 0.1 studied. The ratio of total particle viscosity to fluid viscosity increases at small strains (Fig. 2) because the increase in ratio of PIFS to fluid viscosity is stronger and offsets the decrease in the equivalent ratio of the stresslet. But as the Hencky strain increases, the ratio of the PIFS to the fluid viscosity plateaus and eventually starts to decrease with strain. This, combined with the monotonic decrease of the stresslet ratio, causes the total particle viscosity to decrease relative to the fluid at higher strains. Similar behavior was found for the particle first normal stress coefficient relative to the fluid (including the particle-induced fluid stress and stresslet) in steady shear flow past an isolated sphere [19]. Thus, this nonmonotonicity in a material function is likely to be observed in other linear flows and it is important to understand the physical reasons for its origin.

We develop insight into the PIFS behavior by examining Eulerian contour plots of $C_{kk} - C_{kk}^{f0}$—the difference between polymer conformation trace—at each point in the x_1-x_2 plane and the polymer conformation trace at a far-field point (i.e., with negligible particle effect). Figure 4 shows the contour plots of $C_{kk} - C_{kk}^{f0}$ for the FENE-P model at two different values of strain, $\epsilon = 2$ and $\epsilon = 4$, and Wi $= 0.8$. We see that there are regions of large polymer stretch relative to the fluid, along the principal axis of extension near the particle surface at both the strains considered. However, at larger strains we also observe the presence of blue regions around the particle where the polymer is significantly *less* stretched compared to the polymer stretch in the fluid alone. The stresslet contribution to the suspension viscosity decreases monotonically relative to the fluid as the polymer stretch surrounding a given particle "shields" the particle and thus reduces the local surface tractions. The origin of these regions can be better understood by examining the $\beta \to 1$

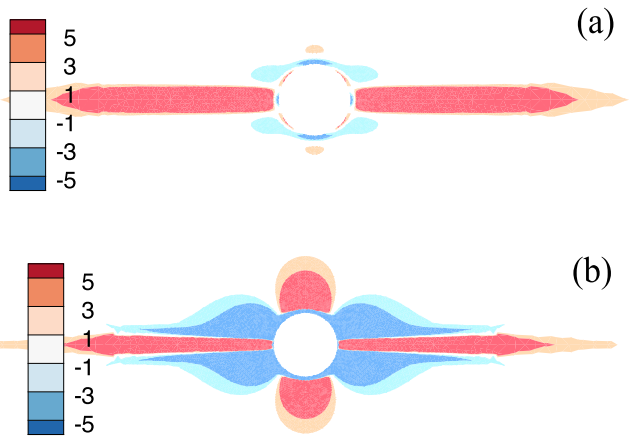

FIG. 4. Eulerian contours of $C_{kk} - C_{kk}^{f0}$ in the x_1-x_2 plane for FENE-P model parameters $L = 100$, $\beta = 0.68$, $\mathrm{Wi} = 0.8$ and strain $\epsilon = 2$ in panel (a) and $\epsilon = 4$ in panel (b).

limit because, in this limit, the flow is approximately Newtonian at all strains and we can thus analyze a known flow field as it effects the polymer evolution [18]. This simplification allows us to characterize the local velocity gradient using a Q-R decomposition [33] and determine the effect of extension- or rotation-dominated regions near the particle surface.

C. Method of characteristics for small polymer concentration $\beta = 1$

We use the method of characteristics [18] to study the polymer response to the local flow field along different streamlines. There is only "one way coupling" from flow to polymer in the $\beta = 1$ limit (meaning the given fixed flow affects the polymer configuration). We solve the set of ordinary differential equations shown below to obtain the polymer conformation along streamlines:

$$\frac{dx_i}{ds} = u_i^N; \quad \frac{dt}{ds} = 1, \tag{23}$$

$$\frac{dC_{ij}}{ds} = C_{ik}\frac{\partial u_j^N}{\partial x_k} + C_{jk}\frac{\partial u_i^N}{\partial x_k} - \frac{1}{\mathrm{Wi}}(C_{ij} - \delta_{ij}), \tag{24}$$

where u_i^N is the Newtonian creeping flow solution for flow past a sphere in uniaxial extensional flow and s is the integration parameter along the streamline.

We show a streamline trajectory in the inset of Fig. 5 that starts far from the particle, and the initial conformation tensor on the streamline is the same as the conformation in the fluid alone at the starting time. We study the evolution of polymer conformation along the same streamline at different dimensionless starting times denoted by ϵ^s for $\mathrm{Wi} = 0.8$. The polymers in the far field get increasingly stretched as time increases and the initial condition for Eq. (24) is different for different starting times. The polymers convected towards the particle get stretched by extension-dominated regions (characterized by $D < 0$) around the particle as shown by points 1 and 2 in Fig. 5. As the polymers enter the vorticity-dominated regions around the particle (characterized by $D > 0$), they lose their alignment with the principal axis of extension and collapse compared to far-field flow. This is shown by points 3 and 4 in Fig. 5. Note that the reduction in polymer stretch (stress) during the collapse (point 4) is far larger than the increase in stretch (stress) through the extension-dominated region. At large distances from the particle denoted by point 5 in the figure, the polymers attain the same configuration as the suspending fluid. The magnitude of polymer stretch and collapse increases as starting times increase because the polymers undergo the coil-stretch transition [5–7] in the far field as time increases. Nearly fully stretched polymers collapse dramatically in rotation regions

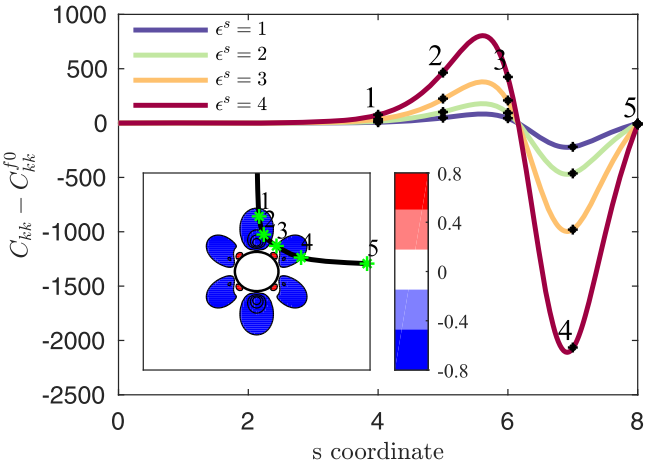

FIG. 5. Evolution of polymer conformation trace along the same streamline at different starting times for Wi = 0.8. Inset shows streamline plotted on top of discriminant D for uniaxial extension flow past a sphere with $D < 0$ indicating extension-dominated and $D > 0$ indicating rotation-dominated regions.

around the particle [34] as shown in Fig. 5. These regions where polymers have significantly smaller stretch compared to the far field contribute negatively to the PIFS and the size of these regions grows around the particle as dimensionless time/strain in the experiment increases. This eventually arrests the growth of the PIFS relative to the fluid, thus it plateaus and decreases at higher strains. From numerical analysis of our flow fields, we claim that these microstructural origins of polymer stretch relative to the suspending fluid for $\beta = 1$ also hold for other β values where the flow field is not Newtonian and the polymer conformation has to be tracked along different time-dependent particle paths for different Wi. The extension- and rotation-dominated regions (characterized by D) also change with time as the flow evolves for $\beta \neq 1$ and it is not easy or necessarily correct to correlate the polymer conformation with the local extension or rotation experienced by the polymer. Therefore, we present the results only for $\beta = 1$.

IV. CONCLUSION

We performed 3D transient simulations of the bulk extensional rheology of dilute particle suspensions for a range of Wi and finite strains and calculated the renormalized per particle extra viscosity of the suspension. We also calculated the particle-induced fluid stress and stresslet contributions analytically for small strain and these calculations agree well with numerical simulations at small strains. We found that the ratio of the per particle extra viscosity to suspending fluid viscosity is nonmonotonic in strain for all constitutive models and for all values of Wi > 0.5 studied. Thus, at a fixed strain, the particle viscosity relative to the fluid may increase or decrease with Wi. The conformation contours show large polymer stretch near the particle in the principal extension direction at modest strains and regions around the particle where the polymers are significantly less stretched compared to the far field at high strains when polymers have undergone coil-stretch transition. These regions grow with strain and thus arrest the PIFS increase relative to the fluid. We believe the nonmonotonicity in ratio of particle viscosity to fluid viscosity is universal for spherical particles in dilute polymer solutions subject to (uniaxial) extensional flow. We look forward to experimental examination of our theoretical predictions in future work.

ACKNOWLEDGMENTS

The authors of this Rapid Communication would like to acknowledge support from NSF (CBET-1803765) and support from the U.S. Army High Performance Computation Research Center

(AHPCRC) with Grant No. W911NF07200271. Computer simulations were also performed on the Stanford University Certainty computer cluster, which is funded by the American Recovery and Reinvestment Act of 2009. A.J. would like to acknowledge financial support from a Stanford Graduate Fellowship. Moreover, J.E. would like to thank the Knut and Alice Wallenberg Foundation for their generous support from a postdoctoral fellowship, KAW 2015.0419.

[1] V. Tirtaatmadja and T. Sridhar, A filament stretching device for measurement of extensional viscosity, J. Rheol. **37**, 1081 (1993).

[2] G. H. McKinley, S. L. Anna, A. Tripathi, and M. Yao, Extensional rheometry of polymeric fluids and the uniaxial elongation of viscoelastic filaments, in *15th International Polymer Processing Society, Netherlands* (1999), Vol. 83.

[3] S. L. Anna, G. H. McKinley, D. A. Nguyen, T. Sridhar, S. J. Muller, J. Huang, and D. F. James, An interlaboratory comparison of measurements from filament-stretching rheometers using common test fluids, J. Rheol. **45**, 83 (2001).

[4] V. Tirtaatmadja and T. Sridhar, Comparison of constitutive equations for polymer solutions in uniaxial extension, J. Rheol. **39**, 1133 (1995).

[5] P. G. De Gennes, Coil-stretch transition of dilute flexible polymers under ultrahigh velocity gradients, J. Chem. Phys. **60**, 5030 (1974).

[6] S. Gerashchenko, C. Chevallard, and V. Steinberg, Single-polymer dynamics: Coil-stretch transition in a random flow, Europhys. Lett. **71**, 221 (2005).

[7] H. P. Babcock, R. E. Teixeira, J. S. Hur, E. S. G. Shaqfeh, and S. Chu, Visualization of molecular fluctuations near the critical point of the coil-stretch transition in polymer elongation, Macromolecules **36**, 4544 (2003).

[8] T. T. Perkins, D. E. Smith, and S. Chu, Single polymer dynamics in an elongational flow, Science **276**, 2016 (1997).

[9] T. T. Perkins, D. E. Smith, R. G. Larson, and S. Chu, Stretching of a single tethered polymer in a uniform flow, Science **268**, 83 (1995).

[10] D. E. Smith and S. Chu, Response of flexible polymers to a sudden elongational flow, Science **281**, 1335 (1998).

[11] R. G. Larson, H. Hu, D. E. Smith, and S. Chu, Brownian dynamics simulations of a DNA molecule in an extensional flow field, J. Rheol. **43**, 267 (1999).

[12] L. Li and R. G. Larson, Comparison of Brownian dynamics simulations with microscopic and light-scattering measurements of polymer deformation under flow, Macromolecules **33**, 1411 (2000).

[13] C. M. Schroeder, E. S. G. Shaqfeh, and S. Chu, Effect of hydrodynamic interactions on dna dynamics in extensional flow: Simulation and single molecule experiment, Macromolecules **37**, 9242 (2004).

[14] A. C. Barbati, J. Desroches, A. Robisson, and G. H. McKinley, Complex fluids and hydraulic fracturing, Ann. Rev. Chem. Biomol. Eng. **7**, 415 (2016).

[15] A. B. Metzner, The mechanics of non-Newtonian fluids: American research and research needs, Rheol. Acta **5**, 65 (1966).

[16] D. L. Koch and G. Subramanian, The stress in a dilute suspension of spheres suspended in a second-order fluid subject to a linear velocity field, J. Non-Newtonian Fluid Mech. **138**, 87 (2006).

[17] K. D. Housiadas and R. I. Tanner, On the rheology of a dilute suspension of rigid spheres in a weakly viscoelastic matrix fluid, J. Non-Newtonian Fluid Mech. **162**, 88 (2009).

[18] D. L. Koch, E. F. Lee, and I. Mustafa, Stress in a dilute suspension of spheres in a dilute polymer solution subject to simple shear flow at finite Deborah numbers, Phys. Rev. Fluids **1**, 013301 (2016).

[19] M. Yang, S. Krishnan, and E. S. G. Shaqfeh, Numerical simulations of the rheology of suspensions of rigid spheres at low volume fraction in a viscoelastic fluid under shear, J. Non-Newtonian Fluid Mech. **233**, 181 (2016).

[20] M. Yang and E. S. G. Shaqfeh, Mechanism of shear thickening in suspensions of rigid spheres in Boger fluids. Part I: Dilute suspensions, J. Rheol. **62**, 1363 (2018).
[21] M. Yang and E. S. G. Shaqfeh, Mechanism of shear thickening in suspensions of rigid spheres in Boger fluids. Part II: Suspensions at finite concentration, J. Rheol. **62**, 1379 (2018).
[22] R. Scirocco, J. Vermant, and J. Mewis, Shear thickening in filled Boger fluids, J. Rheol. **49**, 551 (2005).
[23] S.-C. Dai, F. Qi, and R. I. Tanner, Viscometric functions of concentrated non-colloidal suspensions of spheres in a viscoelastic matrix, J. Rheol. **58**, 183 (2014).
[24] I. E. Zarraga, D. A. Hill, and D. T. Leighton, Jr., Normal stresses and free surface deformation in concentrated suspensions of noncolloidal spheres in a viscoelastic fluid, J. Rheol. **45**, 1065 (2001).
[25] J. Einarsson, M. Yang, and E. S. G. Shaqfeh, Einstein viscosity with fluid elasticity, Phys. Rev. Fluids **3**, 013301 (2018).
[26] W. R. Hwang and M. A. Hulsen, Direct numerical simulations of hard particle suspensions in planar elongational flow, J. Non-Newtonian Fluid Mech. **136**, 167 (2006).
[27] G. D'Avino, P. L. Maffettone, M. A. Hulsen, and G. W. M. Peters, Numerical simulation of planar elongational flow of concentrated rigid particle suspensions in a viscoelastic fluid, J. Non-Newtonian Fluid Mech. **150**, 65 (2008).
[28] M. Ahamadi and O. G. Harlen, Numerical study of the rheology of rigid fillers suspended in long-chain branched polymer under planar extensional flow, J. Non-Newtonian Fluid Mech. **165**, 281 (2010).
[29] G. K. Batchelor, The stress system in a suspension of force-free particles, J. Fluid Mech. **41**, 545 (1970).
[30] E. J. Hinch, An averaged-equation approach to particle interactions in a fluid suspension, J. Fluid Mech. **83**, 695 (1977).
[31] A. Einstein, Eine neue bestimmung der moleküldimensionen, Ann. Phys. (Berlin, Ger.) **324**, 289 (1906).
[32] A. Einstein, Berichtigung zu meiner arbeit: Žeine neue bestimmung der moleküldimensionen, Ann. Phys. (Berlin, Ger.) **339**, 591 (1911).
[33] M. S. Chong, A. E. Perry, and B. J. Cantwell, A general classification of three-dimensional flow fields, Phys. Fluids A: Fluid Dyn. **2**, 765 (1990).
[34] E. S. G. Shaqfeh, G. H. McKinley, N. Woo, D. A. Nguyen, and T. Sridhar, On the polymer entropic force singularity and its relation to extensional stress relaxation and filament recoil, J. Rheol. **48**, 209 (2004).